Journal of the Korean Nuclear Society
Volume 33, Number 3, pp.327~338, June, 2001

Flow Analysis for Optimum Design of Mixing Vane in a PWR Fuel Assembly

Wang Kee In, Dong Seok Oh, and Tae Hyun Chun
Korea Atomic Energy Research Institute
150 Dukjin-dong, Yusong-gu, Taejon 305-353, Korea
wkin@kaeri.re.kr

(Received January 2, 2001)

Abstract

A computational fluid dynamics (CFD) analysis was performed to propose the optimum design of flow mixing vane on the space grid in a PWR fuel assembly. The flow mixing vanes considered in this study for optimum design are swirl-vane and twisted-vane. A single subchannel of one grid span was modeled using flow symmetry to minimize the computational effort. The CFD predictions are in good agreement with the experimental results for the split-vane, which shows the applicability of the CFD method. The mixing effect by swirling flow and crossflow, and the pressure drop were estimated and compared for the various vane angles. The optimum vane angle is proposed to be 40° and 35° from the direction of axial flow for the swirl-vane and the twisted-vane, respectively.

Key Words : mixing vane, subchannel, vane angle, swirl, CFD

1. Introduction

The fuel assembly typically used in PWR nuclear reactors is a square rod bundle whose rod-to-rod clearance is maintained by the grid. The coolant moves axially through the subchannels formed between neighboring fuel rods and between the peripheral fuel rods and the flow tube. The fuel spacer affects the coolant flow distribution in the fuel rod bundle, and so the spacer geometry has a strong influence on a bundle' s thermal-hydraulic characteristics, such as the critical heat flux and pressure drop. Attempts have been made to increase the departure from nucleate boiling (DNB) performance by providing the support grid structures employed to contain the members of the fuel assembly with integral flow deflecting vanes. These vanes can improve the DNB performance by increasing coolant mixing and the rod heat transfer ability downstream of the vanes. These attempts to improve performance have been met with varying success depending on the vane design and the design of the other grid components, which can have an impact on the effectiveness of the vanes.

To maximize the benefit of the vanes, their size, shape, bend angle, and location must be optimized. It is therefore essential to evaluate the

three-dimensional flow characteristics in detail for the optimum design of the space grid with flow mixing vanes. Since the optimum spacer design should consider a large number of shapes and sizes of mixing blades on the grid spacer, the utilization of the CFD (Computational Fluid Dynamics) method is inevitable to sift better fuel-spacer designs for the final experimental verification.

A prediction of the detailed structure of the turbulent flow in the rod bundles, used especially as nuclear fuel elements, is required to ensure their safe and reliable operation. The experimental data on flow mixing between the subchannels of bare rod bundles [1-3] showed that the periodical flow pulsations between subchannels are the main mechanisms for the natural mixing between subchannels resulting from radial pressure gradients between adjacent subchannels. The presence of the space grid and flow mixing devices causes the forced mixing of coolant that promotes flow mixing either within a subchannel or between subchannels. Shen et al. [4] investigated the cross-flow mixing effect caused by the grid spacer with ripped-open blades. They measured the cross-flow velocity and the RMS velocity at the rod gap region depending on the angle of the mixing blade on the grid spacer. Karoutas et al. [5] performed a 3-D flow analysis for the design of a nuclear fuel spacer with the mixing devices by CFD and experimental methods. Yang and Chung [6] measured turbulent flow characteristics in the subchannels of a 5x5 rod bundle with split-vane and found that turbulent mixing and forced mixing occurs behind the space grid. Imaizumi et al. [7] developed a CFD method to evaluate the 3-D flow characteristics for a PWR fuel assembly in order to improve the design approach. In et al. [8] and In [9] also showed that the CFD analysis represented well the characteristics of turbulent flow in the nuclear fuel bundle with the mixing vanes on the space grid and therefore could be quite useful for the optimum design of an advanced flow mixing device.

A CFD analysis was performed to propose the optimum design of flow mixing vanes (swirl-vane and twisted-vane) on the space grid in a PWR fuel assembly. This paper also presented the CFD simulations of the 5x5 rod bundle experiments with split-vane [5, 6] to illustrate the applicability of the CFD method.

2. Flow Mixing Vanes

The split-vane design in Fig. 1(a) is to provide vanes that are integrally formed on the upper

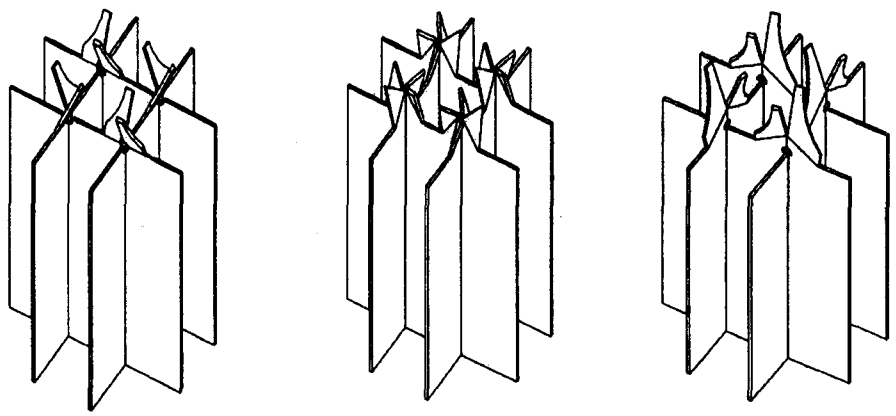

Fig. 1. Grid Spacer Designs; (a) Split-vane, (b) Swirl-vane, and (c) Twisted-vane

edges of the interlaced straps of a grid, and bent over in the flow channel so as to deflect the upwardly flowing coolant. The vanes are formed in pairs with a slit and recess between them, such that each vane can be bent in an opposite direction. This design was optimized for size, strength and corrosion resistance. The split-vane was used in the experiments of Karoutas et al. [5] and Yang and Chung [6]. The vane angle bent from the vertical axis is generally between 20° and 30°. The bent vanes deflect the coolant to mix between the subchannels of the spaced parallel fuel rods or to swirl within the subchannel.

The swirl-vane was invented to generate a strong swirling flow in the subchannel. It is designed to provide a fuel space grid with swirl vanes each capable of generating a strong swirl like an air vane as shown in Fig. 1(b). The space grid includes four swirl deflectors provided at the upper ends of the interconnections between the straps. The swirl deflectors have an air vane structure including blades that are configured to have the same vane rotation direction. Each swirl vane has a pair of intersecting triangular base plates extending upwardly from the interconnecting straps. The swirl vanes are bent in the same direction from the associated side base plates. This design results in a small blocking area of flow and thereby minimizes the loss of pressure caused by the flow deflectors.

The space grid with a twisted-vane illustrated in Fig. 1(c) shows two mixing vanes at the upper ends of the interconnections between the straps which are bent in opposite direction at the top slope of the triangular base. This is the modified design of the swirl-vane to generate a crossflow between the subchannels as well as a swirling flow in the subchannel by directing the coolant simultaneously to the fuel rod and the rod gap. The twisted-vane with a smooth change of the flow area also complements the split-vane design with an abrupt change of the flow area that deflects the coolant directly to the gap.

3. Numerical Method

3.1. Geometry Modeling

A single subchannel of one grid span is modeled using flow symmetry by a CFD code, CFX [10]. The spacer and mixing vanes are treated as infinite thin surfaces. The other fuel spacer elements such as the spring and arches are neglected for simplicity because their effect on the flow mixing is judged to be minimal only inside and near the spacer. The three-dimensional CFD

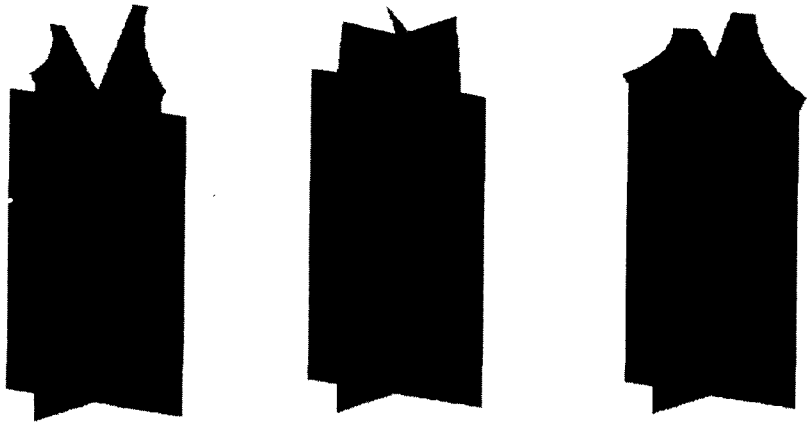

Fig. 1. Grid Spacer Designs; (a) Split-vane, (b) Swirl-vane, and (c) Twisted-vane

models are developed by a structured multi-block method. The size of the mixing vanes was assumed based on engineering judgment. The vane angle (θ), defined as the angle bent from the axial direction, was assumed to be 25° for split-vane from the above experimental works. The vane angle changed from 25° to 45° and from 25° to 40° for the swirl-vane and the twisted-vane, respectively.

Fig. 2 illustrates the partial views of the structured CFD models of the space grids with various mixing vanes. The numerical simulation starts 65 mm upstream and 500 mm downstream of the top of the space grid, which is similar to the grid span used in the related experiements [5, 6]. The split-vane model was structured with 180 blocks and about 247000 cells. This model is to simulate the laser Doppler velocimeter(LDV) experiments of Karoutas et al. [5] and Yang and Chung [6]. The swirl-vane model was built with 100 blocks and 224000 cells. The twisted-vane model was created with 96 blocks and approximately 250000 cells.

Fig. 3 shows the computational grids of a cross-section of the single subchannel. The computational grids are 32x34x256 (split-vane), 36x36x245 (swirl-vane), and 30x32x245 (twisted-vane). The computational grid used at the rod gap is 16 or 18. The computational grid test was conducted with the split-vane case for 16x16x256, 24x24x256 and 32x34x256 cells. The case with 32x34x256 cells resulted in the most reasonable predictions. A fine grid was used near the grid spacer and the rod surfaces. The grid size in non-dimensional wall unit (y^+) was calculated to be 15-50 for all cases, which is the closest distance from the rod surface. A non-uniform grid was also used in the axial direction with the fine grid near the inlet boundary and the mixing vanes, and the coarse grid near the outlet boundary. The axial length of the cells varied from 0.15 - 0.3 mm at the mixing vane to 4.1-7.0 mm near the end of the CFD model.

3.2. Boundary Conditions

The inlet boundary conditions used in these simulations were taken from a model without a space grid. Velocities, turbulent kinetic energy and turbulent dissipation rate were transferred from the outlet in the no spacer case to the inlet in the simulations with spacers. A constant pressure condition was applied at the outlet boundary. A special periodic boundary condition at the rod gap regions was used to model the crossflow between neighboring subchannels and reduce the size of the computational model. What is coming out through one side boundary is going in through

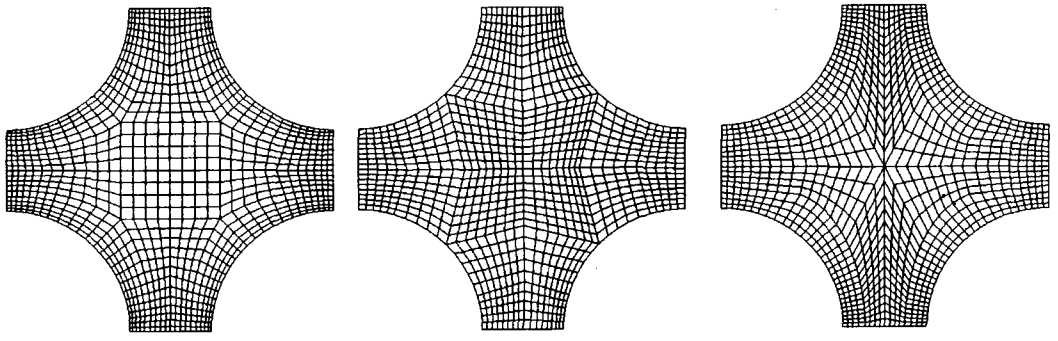

Fig. 3. Computational Grids of a Cross-section of the Single Subchannel for Split-vane (left), Swirl-vane (middle), and Twisted-vane (right)

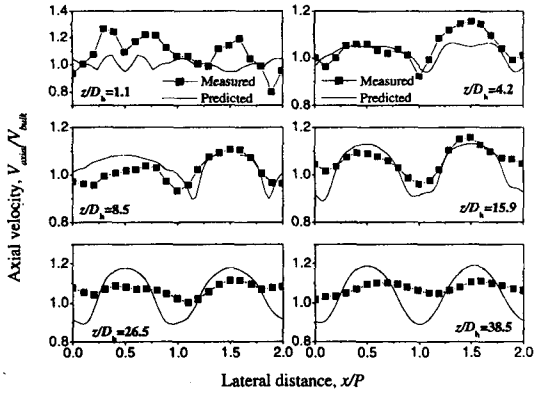

Fig. 4. Comparison of Axial Velocity Along the Centerline of the Subchannel for a Split-vane

another side boundary in the computational model. A no-slip condition was used at the rod surface and the grid spacer.

3.3. Numerical Analysis

Karoutas et al. [5] conducted an experiment in a full-scale cold water loop for a 5x5 rod array test section with the split-vane on the space grid. The working fluid is water and the bulk inlet velocity (V_{bulk}) is 6.79 m/sec (Re=85000). They reported the axial and lateral velocity measurements taken at the centerline across adjacent subchannels for the split-vane design. Yang and Chung [6] also carried out a similar experiment for the split-vane, and reported the measurements of axial velocity and turbulent intensity in the subchannel. These experimental conditions were used in this numerical study.

The standard k-ϵ turbulence model of Launder and Spalding [11] was used in the current CFD analysis since it is practically useful and converges well for the complex turbulent flow in a nuclear rod bundle. A standard under-relaxation method and hybrid difference scheme were used to obtain a converged solution. The calculation was performed on an HP9000 C200 workstation (PA8000 CPU, 512 MB RAM) and terminated when the residual for the mass equation (sum of the absolute values of the net mass flux into or out of every cell in the flow field) is less than approximately 10^{-4} kg/s. The total inlet mass flow rate is 0.6 kg/s. Approximately 5000 iterations (~100 hrs) were necessary to obtain a converged solution.

4. Results and Discussions

4.1. Comparison with Experimental Results

The CFD predictions for the split-vane were compared with the experimental results of Karoutas et al. [5] and Yang and Chung [6]. The axial and lateral mean velocities were predicted along the centerline of the subchannel and compared to the measurements of Karoutas et al. The uncertainty in the velocity measurements was determined to be within a range of 0.1% to 0.5%. Fig. 4 shows the comparison of the axial velocity (V_{axial}) along the horizontal and vertical centerlines of the subchannel downstream of the space grid with a split-vane. The horizontal centerline ranges from x/P=0.0 to x/P=1.0 and the vertical centerline from x/P=1.0 to x/P=2.0 in Fig. 4. The symbols P and D_h are the rod array pitch and the hydraulic diameter of a subchannel, respectively. The velocity is normalized by the bulk velocity of the subchannel (V_{bulk}=6.79 m/sec).

There are some significant differences between the predictions and the measurements close to the spacer. These larger differences are possibly due to the assumption of infinite thin spacer strap and no rod support features of the spacer such as springs and arches. The comparison shows qualitatively good agreement further downstream of the spacer ($z/D_h \geq 8.5$). It is noted that the distribution of axial velocity develops to the

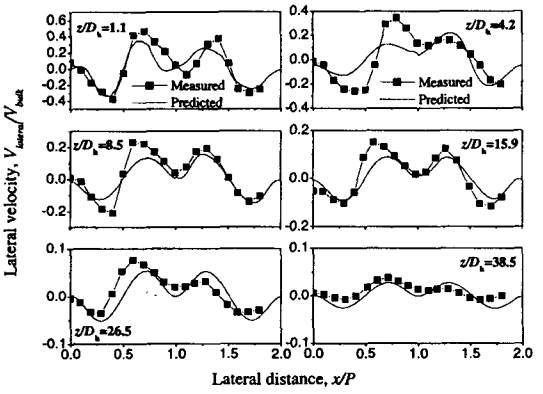

Fig. 5. Comparison of Lateral Velocity Along the Centerline of the Subchannel for a Split-vane

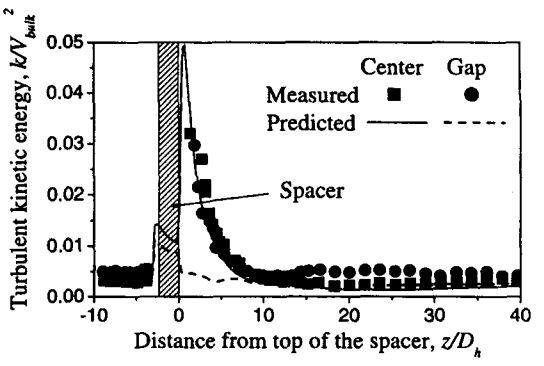

Fig. 6. Comparison of Turbulent Kinetic Energy in the Subchannel for a Split-vane

parabolic profile in both measurements and predictions. Far downstream (z/D_h=38.5), the predicted axial velocities show a more developed (parabolic) shape than the measurements show. This may be due to not modeling the next spacer at the outlet of the CFD model. The next spacer was not modeled to minimize the size and execution of the CFD simulation. The next spacer would have a damping effect on the centerline subchannel velocity.

Fig. 5 shows the comparison of the lateral velocity ($V_{lateral}$) along the horizontal and vertical centerlines of the subchannel for the split-vane design. It can be seen that the lateral velocity produced by the split-vane is high close to the spacer but decreases significantly further downstream. The maximum lateral velocity is larger than 30% of the bulk velocity at z/D_h=1.1 and reduces to smaller than 5% at z/D_h=38.5. The lateral velocity along the horizontal centerline ($0.0 \leq x/P \leq 1.0$) is somewhat under-predicted and the lateral velocity along the vertical centerline ($1.0 \leq x/P \leq 2.0$) shows good agreement. These discrepancies appear to be caused mainly by inexact dimension of the split-vane. Modeling of multi-subchannels would somewhat enhance the accuracy of the predictions as well. In general, the CFD results are judged to reasonably present the characteristics of coolant flow mixing in the subchannel caused by a split-vane.

Fig. 6 shows the variation of turbulent kinetic energy at the center of the subchannel and the rod gap for the split-vane design. The predicted results are also compared with the experimental results reported by Yang and Chung [6]. The measured kinetic energy was estimated from the measured axial turbulent intensity assuming isotropy. The CFD predictions indicate a significant increase in the turbulent kinetic energy at the leading edge of the spacer. The turbulent kinetic energy predicted at the center of the subchannel increased again due to the acceleration of flow by the split-vane on the top of the spacer. Even though the turbulent kinetic energy is somewhat under-predicted, the agreement with the measurements appears to be reasonable. A large discrepancy can be noted at the gap where a strong anisotropy of turbulence is known to occur. However, this CFD analysis used the standard k-ε model that assumes isotropic turbulence. The measured kinetic energy at the gap also appeared to be overestimated from the axial turbulent intensity because the isotropic assumption was used.

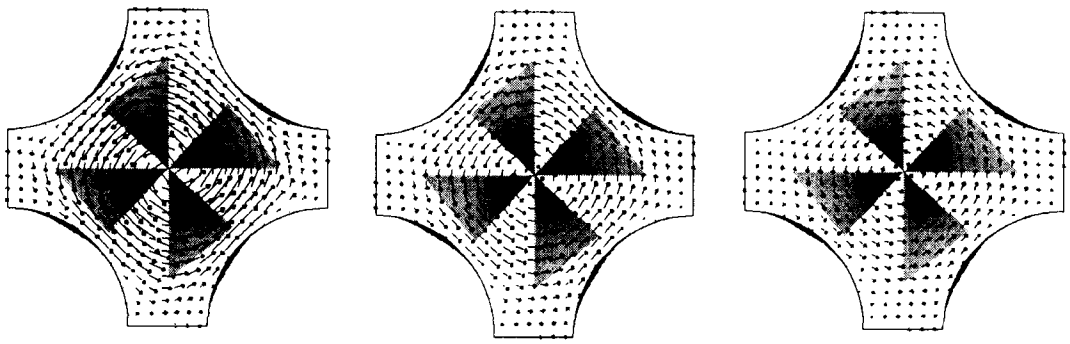

Fig. 7. Velocity Vectors in the Subchannel for a Swirl-vane with a Vane Angle of 40° at z=2D_h (left), z=10D_h (middle), z=20D_h (right)

4.2. Optimum Design of Flow Mixing Vane

A swirl-mixing ratio in the subchannel is defined to estimate the coolant mixing effect of the mixing vane as

$$S_M = \frac{\int r^2 V_{lateral} U dr}{R_S \int r U^2 dr}. \quad (1)$$

The symbols U and r are the local axial velocity along the centerline of the subchannel and the horizontal or vertical distance from the center of the subchannel, respectively. The symbol R_S is the radius of swirl that is defined as a normal distance from the center of the subchannel to the rod surface. The swirl-mixing ratio (S_M) was calculated at various locations downstream of the spacer.

The amount of crossflow mixing is evaluated by integrating the absolute transverse velocity (V_{cross}) across a rod gap as

$$F_{CM} = \frac{1}{s} \int \frac{|V_{cross}|}{V_{bulk}} dy. \quad (2)$$

The symbol s indicates the gap distance. Increasing the swirl mixing ratio and the cross-flow mixing, and their persistence downstream of the spacer is believed to improve DNB performance. The axial variation of average turbulent kinetic energy in the subchannel is also examined to evaluate the flow mixing by turbulence caused by the mixing vane.

Another important factor in the optimum design of the mixing vane is the pressure drop across the space grid with the mixing vane. The mixing vane should be optimized in order to minimize the additional pressure loss as well as to maximize the coolant mixing. The pressure distributions predicted in this CFD analysis are not accurate because the thickness of the spacer and the mixing vanes, and the spacer components such as the spring and dimple were neglected in the current CFD models. However, it is relevant to compare the pressure variations due to the acceleration and/or deceleration of flow caused by the mixing vane. The additional pressure drop (Δp) is defined as

$$\Delta p = \frac{\Delta p(\theta) - \Delta p(no\ vane)}{\Delta p(no\ vane)}. \quad (3)$$

4.2.1. Swirl-Vane Design

The swirl-vane produces a circular swirling flow in the subchannel and an insignificant crossflow between the subchannels as illustrated in Fig. 7. A

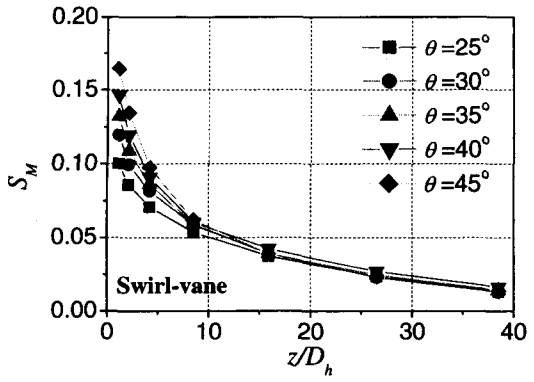

Fig. 8. Axial Variation of Swirl-mixing Ratio in the Subchannel for a Swirl-vane

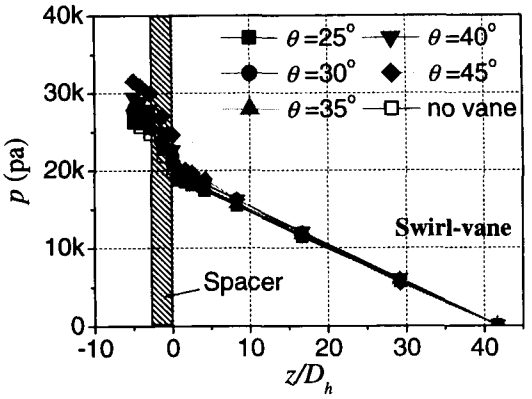

Fig. 10. Pressure Distribution in the Subchannel for a Swirl-vane

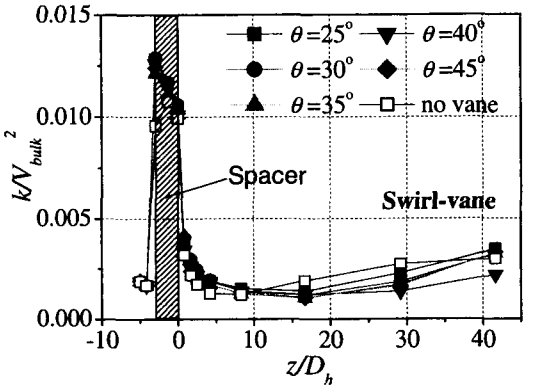

Fig. 9. Axial Variation of Average Turbulent Kinetic Energy in the Subchannel for a Swirl-vane

strong swirl is predicted to occur near the spacer ($z=2D_h$) and slowly decays downstream of the spacer ($z=10D_h$, $20D_h$). The swirl keeps the same direction of rotation downstream of the spacer. The CFD prediction showed that the swirling flow changes to axially dominant flow further downstream.

Figure 8 shows axial variation of the swirl-mixing ratio downstream of the spacer for different vane angles. It indicates an intense coolant mixing near the spacer caused by the mixing vane and an exponential decay of the swirl mixing. A significant mixing apparently persists to 15-20 times the hydraulic diameter of the subchannel ($z=15$-$20D_h$) downstream of the spacer. The swirl mixing ratio increases as the vane angle increases. The swirl mixing at $\theta=45°$, except the region close to the spacer ($z<10D_h$), appears to be smaller than that at $\theta=40°$. This might be caused by a direct deflection of coolant onto the rod surface at such a large vane angle of 45°. The flow impingement would reduce the strength of the swirl in the subchannel.

The average turbulent kinetic energy in the subchannel shown in Fig. 9 increases significantly in the spacer region and rapidly decreases downstream of the spacer. It shows practically the same level of turbulent kinetic energy independent of the vane angle and even similar to the case without the vane ten(10) times the hydraulic diameter downstream. In other words, the swirl-vane effect on subchannel turbulence seems to disappear within $10D_h$ downstream.

Figure 10 shows the pressure distributions in the subchannel for various vane angles. The pressure appears to rapidly decrease across the spacer and slightly increase right downstream of the spacer due to the flow deceleration. It shows a gradual increase of the pressure drop in the subchannel as the vane angle increases. The additional pressure

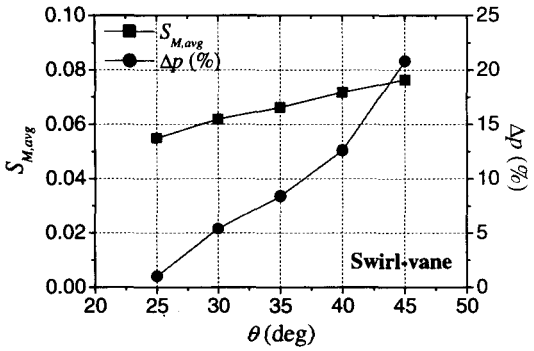

Fig. 11. Effect of Vane Angle on the Swirl-mixing Ratio and the Pressure Drop for a Swirl-vane

drop defined as eq.(3) was estimated to be 1.02%, 5.4%, 8.4%, 12.6%, and 20.8% for θ = 25°, 30°, 35°, 40°, and 45°, respectively. It is noted that a larger pressure drop occurs between θ = 40° and θ = 45°.

As stated above, the swirl-vane was predicted to neither generate a distinctive crossflow, nor increase the turbulent kinetic energy persisting far downstream of the spacer. Hence, the average swirl-mixing ratio ($S_{M,avg}$) and the additional pressure drop (Δp) for the swirl-vane case are plotted in Fig. 11 as a function of the vane angle. The average swirl-mixing ratio continually increases as the vane angle increases. However, as shown in Fig. 8, the swirl-mixing ratio at =45° appears to rapidly decrease downstream of the spacer and is even smaller than the case at =40° far downstream. Fig.11 also shows an increase of the pressure drop with the increase of vane angle. As already noted in Fig.10, a significantly large pressure drop is predicted to occur above a vane angle of 40°.

4.2.2. Twisted-Vane Design

Figure 12 illustrates the velocity vector in the subchannel at various locations downstream of the spacer. The twisted-vane forms a skewed elliptic swirling flow and a significant crossflow at $z=2D_h$. The flow pattern changes to the circular swirl similar to that of the swirl-vane and a mild cross-flow remains at $z=10D_h$. A slight counter-current crossflow seems to occur near $z=10D_h$. The swirling flow in the subchannel persists far downstream but the crossflow between the subchannels diminishes approximately at $z=20D_h$.

Figure 13 shows the effect of the vane angle on the swirl-mixing ratio. It indicates an intense coolant mixing near the spacer caused by the twisted-vane and an exponential decay of forced mixing downstream. The coolant mixing by the swirling flow is predicted to significantly increase near the spacer as the vane angle increases. It is also noted that swirl mixing appears to be

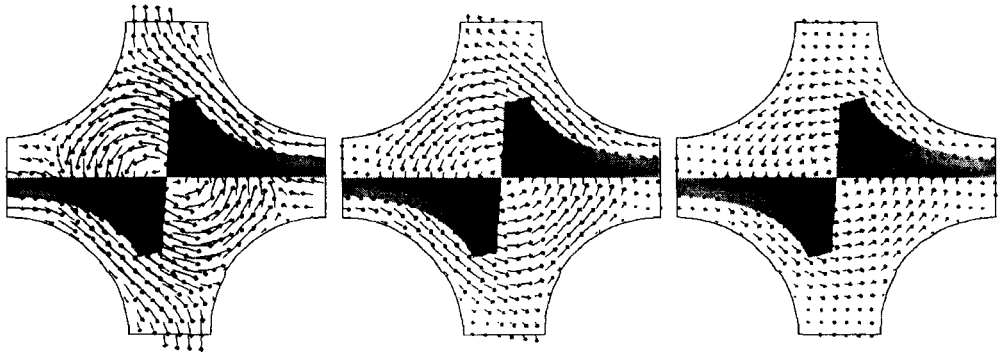

Fig. 12. Velocity Vectors in the Subchannel for a Twisted-vane with a Vane Angle of 35° at $z=2D_h$ (left), $z=10D_h$ (middle), $z=20D_h$ (right)

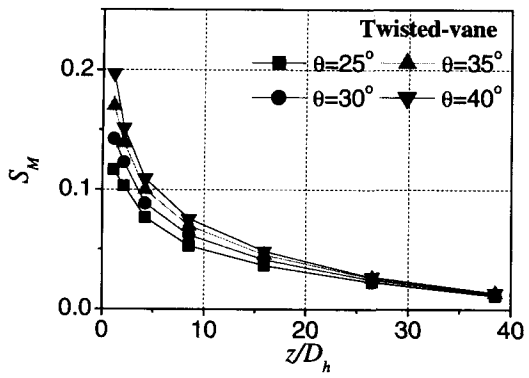

Fig. 13. Axial Variation of Swirl-mixing Ratio in the Subchannel for a Twisted-vane

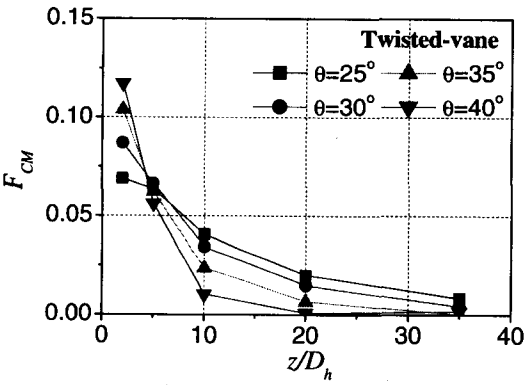

Fig. 14. Axial Variation of Crossflow-mixing Factor in the Subchannel for a Twisted-vane

independent of the vane angle approximately $20D_h$ downstream of the spacer. Figure 14 shows the axial variation of the crossflow-mixing factor (F_{CM}) estimated by eq. (2). The crossflow increases significantly close to the spacer ($z<5D_h$) and rapidly decreases further downstream as the vane angle increases. The crossflow mixing at the vane angle of 40° appears to be negligible ten times the hydraulic diameter downstream of the spacer.

Figure 15 shows the axial variation of average turbulent kinetic energy in the subchannel for various vane angles. Similar to the swirl-vane case, the turbulent kinetic energy rapidly decreases

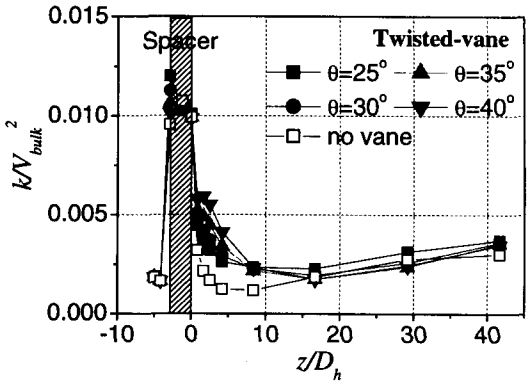

Fig. 15. Axial Variation of Average Turbulent Kinetic Energy in the Subchannel for a Twisted-vane

downstream of the spacer. Turbulence generated by the mixing vane seems to increase very close to the spacer ($z<5D_h$) as the vane increases. The pressure distribution across the space grid in Fig. 16 shows a gradual increase of the pressure drop in the subchannel as the vane angle increases. The additional pressure drop defined as eq.(3) was estimated to be 11.8%, 17.0%, 22.8%, and 29.5% for =25°, 30°, 35°, and 40°, respectively. The increase of pressure drop is mainly due to larger flow blocking area of mixing vane as the vane angle increases.

Figure 17 shows the variations of average swirl-mixing ratio ($S_{M,avg}$), average crossflow-mixing factor ($F_{CM,avg}$) and the additional pressure drop (Δp) for the twisted-vane case as a function of the vane angle. The average crossflow-mixing factor was estimated as the mean value of significant crossflow factors up to $10D_h$. The swirl mixing and the pressure drop are predicted to continually increase as the vane angle increases. The pressure drop is higher than 25% at θ=40° due to large flow blocking area that is 26.3% of total subchannel area. The average crossflow-mixing factor appears to decrease above a vane angle of 35° because the crossflow at large vane angle

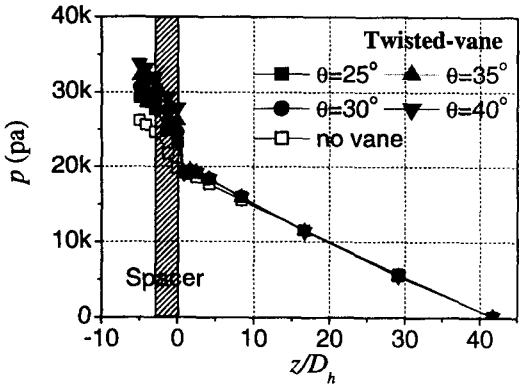

Fig. 16. Pressure Distribution in the Subchannel for a Twisted-vane

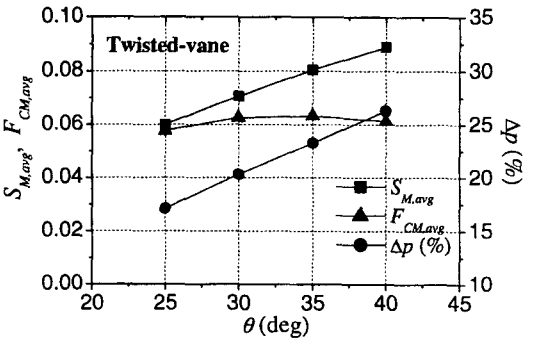

Fig. 17. Effect of Vane Angle on the Swirl and Crossflow Mixing, and the Pressure Drop for a Twisted-vane

rapidly decreases downstream of the spacer as shown in Fig. 14.

5. Conclusions

A series of CFD analyses were performed to illustrate the applicability of the CFD method and assess the effect of the mixing-vane angle bent from the axial flow direction in a PWR fuel assembly. The CFD simulation of the rod bundle experiment with a split-vane showed good agreement with the measurements of axial and lateral mean velocities, and turbulent kinetic energy. The CFD analyses show that the swirl and the crossflow by the mixing vane is the dominant flow mixing mechanism in a rod bundle. For the swirl-vane design, the swirl mixing with a negligible crossflow mixing appears to rapidly decrease downstream of the spacer and a significantly large pressure drop is predicted to occur above a vane angle of 40°. For the twisted-vane design, the crossflow mixing tends to decrease and the pressure drop is also very large above a vane angle of 35°. The optimum vane angle is therefore judged to be 40° and 35° for the swirl-vane and the twisted-vane, respectively. Finally, it is believed that an advanced mixing vane for higher DNB performance should be designed to generate a strong swirl and crossflow without causing an excessive pressure drop.

Acknowledgement

The author expresses his appreciation to the Ministry of Science and Technology (MOST) of Korea for financial support.

References

1. D. S. Rowe, B. M. Johnson and J. G. Knudsen, " Implications Concerning Rod Bundle Crossflow Mixing Based on Measurements of Turbulent Flow Structure," *International Journal Heat Mass Transfer*, **17**, 407 (1974).
2. S. V. Moller, "On Phenomena of Turbulent Flow through Rod Bundles," *Experiments in Thermal and Fluid Science*, **4**, 25 (1991).
3. K. Rehme, "The Structure of Turbulence in Rod Bundles and the Implications on Natural Mixing Between the Subchannels," *International Journal of Heat and Mass Transfer*, **35**, 567 (1992).
4. Y. F. Shen, Z. D. Cao and Q. G. Lu, "An Investigation of Crossflow Mixing Effect Caused

by Grid Spacer with Mixing Blades in a Rod Bundle," *Nuclear Engineering and Design*, **125**, 111 (1991).

5. Z. Karoutas, C. Y. Gu and B. Scholin, "3-D Flow Analyses for Design of Nuclear Fuel Spacer," *Proc. of the 7th International Meeting on Nuclear Reactor Thermal-Hydraulics*, New-York, United Sates, September, (1995).
6. S. K. Yang and M. K. Chung, "Spacer Grid Effects on Turbulent Flow in Rod Bundles," *Journal of the Korean Nuclear Science*, **28**, 56 (1996).
7. M. Imaizumi, T. Ichioka, M. Hoshi, H. Teshima, H. Kobayashi and T. Yokoyama, "Development of CFD Method to Evaluate 3-D Flow Characteristics for PWR Fuel Assembly," *Trans. of the 13th International Conference on SMiRT*, Porto Alegre, Brazil, August, 1995.
8. W. K. In, D. S. Oh, T. H. Chun and Y. H. Jung, "Numerical Examination of Coolant Flow Mixing in Nuclear Fuel Assembly with Mixing Promoters", *8th Int. Conference on Nuclear Engineering*, Baltimore, USA, April 2-6 (2000).
9. W. K. In, "Numerical Study of Coolant Mixing Caused by the Flow Deflectors in a Nuclear Fuel Bundle," *Nuclear Technology*, **134** (2), 187(2001).
10. CFX International, CFX-4.2: Solver, AEA Technology, Oxfordshire, UK (1997).
11. B. E. Launder and D. B. Spalding, "The Numerical Computation of Turbulent Flows," *Computational Methods in Applied Mechanics and Engineering*, **3**, 269 (1974).